RSC Advances

RSC Advances

www.rsc.org/advances

ROYAL SOCIETY OF CHEMISTRY

www.rsc.org/advances

1   *In vivo* cytotoxicity of MgO-doped nanobioactive glass particles and their anticorrosive
2   coating on Ti-6Al-4V and SS304 implants for high load-bearing applications

3   M. Prabhu[a], R. Suriyaprabha[a], V. Rajendran[a]*, P. Kulandaivelu[b], and S. Valiyaveettil[c]

4   [a]Centre for Nano Science and Technology, K. S. Rangasamy College of Technology,
5   Tiruchengode – 637215, Tamil Nadu, India.
6
7   [b]Department of Mechanical Engineering, K. S. Rangasamy College of Technology,
8   Tiruchengode – 637215, Namakkal (Dt.), Tamil Nadu, India.
9
10   [c]Department of Chemistry, Faculty of Science, National University of Singapore, 3
11   Science Drive 3, Singapore-117543.
12

13   **Abstract**

14   In this study, magnesium-doped nanobioactive glass (NBG) composites (SiO_2–CaO–

15   P_2O_5–MgO) were prepared by simple sol–gel method, which were characterized and coated

16   on Ti alloy (Ti-6Al-4V) and stainless steel (SS304) implants by spin-coating technique. The

17   prepared nanocomposite shows amorphous nature and spherical morphology with particle

18   size of less than 100 nm. The adsorption and desorption isotherms showed the prepared

19   nanocomposites to be in mesoporous range with a specific surface area of 104.1 m^2g^{-1}. The

20   coated implant was found to have a uniform structure without any cracks and pores.

21   Magnesium-doped NBG-coated Ti implants show high corrosion resistance and hardness. In

22   addition, formation of bone-like apatite layer on the coated implant was found to be high in

23   magnesium-doped NBG particles. In addition, *in vivo* toxicity of the glasses was studied in

24   zebrafish (*Danio rerio*) embryos, and the results confirmed significant toxicity at higher

25   concentration. Hence, Magnesium-doped NBG-coated implant is found to be a potential

26   nanocomposite for high load-bearing applications with better anticorrosive property and long-

27   term stability.

28   *Address for correspondence: veerajendran@gmail.com
29   Tel.: +91-4288-274741-4, 274880
30   Fax: +91-4288-274880 (direct), 274860

1   **Introduction**

2   Metallic implants such as pure titanium (Ti), titanium alloys (Ti-6Al-4V), and

3   stainless steels (SS 316L) are widely for orthopedic and high load bearing

4   applications.[1–5] When an implant is inserted inside the human body, it may weaken the

5   surrounding bone and cause failure between bone and implants due to microbial

6   infections.[4,5] To resolve this problem, most of the researchers are interested in

7   developing calcium- and phosphate-based ceramic-coated implant to induce

8   osteoconductive properties along with antimicrobial activity.[6–8] A review of previous

9   studies has shown that limited work has been conducted on the fabrication of a

10   composite coating of bioactive glass (BG) and Ti-6Al-4V for biomedical implants. [2,9–

11   [12] In this regard, many coating methodologies such as plasma spraying[13], pulsed laser

12   deposition[14], and dip-coating[1] have been adapted. However, the area of efficiency and

13   durability of coated materials on implant is interesting and still to be explored. Spin

14   coating of porous silicon- and zinc-doped hydroxyapatite (HAp) on SS implants may

15   enhance their adhesiveness and long-term durability[15,16], which are favorable for bone

16   implant applications.

17   In fact, for improved osteogenic properties, coating of antimicrobial and

18   biocompatible nanobioactive glass (NBG) particles should be used on implants to

19   expand the application of NBG for high load-bearing applications.[17] HAp sprayed on

20   the implant surface as a bioactive coating material has few drawbacks in terms of

21   adherence to the metal substrate. For example, HAp coating on titanium implant

22   surfaces may result in rough surface and increase osseointegration, but its adherence to

23   the metal is not perfect.[18] Bioglass may be known to act as a better osteoproductive,

24   abrasive, and highly resorbable surface material for implants[17,19], but extensive

1   investigations are required to explore the bioactive glass coating as an active

2   biomaterial on clinical implants.

3   The NBGs are coated on glass films to explore higher bioactivity.[20] However, it

4   is found that chemical composition and microstructure of the glass particles have an

5   important role in implant applications. Hence, the glass composition that possesses

6   optimal physicochemical properties and better *in vitro* biocompatibility is used for the

7   implant-coating applications. Our earlier investigations on the development of NBG

8   composites prepared with Mg, Ag, and Zr show the *in vitro* bioactivity of the material

9   for biomedical applications.[21,22] Among the glass compositions tested, the one with 10

10   % Mg was found to possess the required mechanical and physicochemical properties.

11   Hence, the coating of Mg-doped NBG particles on implant materials led to desirable

12   biomimetic characteristics for high load-bearing applications.

13   The screening of the *in vivo* toxicity of the optimized Mg-doped NBG (SiO_2–

14   CaO–P_2O_5–MgO) particles is mandatory for any implant coating. In this regard, a

15   zebrafish model can be used to analyze the biocompatibility and *in vivo* cytotoxicity of

16   the prepared glass compositions. As the genotype of zebrafish is closely similar to the

17   human genotype[23], the analysis of toxicity in fish enables us to understand the human

18   health risks of novel biomaterials. In addition, large quantity of zebrafish embryos can

19   be developed rapidly at low cost, which serves as an inexpensive and faster *in vivo*

20   assay to screen the biocompatibility, pharmacological efficacy, and toxicity of

21   biomaterials.

22   This study aimed to examine the *in vivo* cytotoxicity of Mg-doped NBG (SiO_2–

23   CaO–P_2O_5–MgO) particles in zebrafish (*Danio rerio*) embryos and to coat these

24   particles on implant materials such as Ti alloy (Ti-6Al-4V) and stainless steel (SS304)

1   plates using spin-coating technique. In addition, this study aimed to explore the *in*

2   *vitro* bioactivity using simulated body fluid (SBF), and to explore the mechanical and

3   anticorrosive properties using artificial saliva on the coated implants.

4   **Results and discussion**

5   **Characterization of prepared Mg-doped NBG particles**

6   The XRD pattern of the synthesized Mg-doped NBG particles shows amorphous

7   nature as no diffraction peaks are observed except a broad band between 10° and 35°

8   (Fig. 1a). TEM images showed that Mg-doped NBG particles possess uniform

9   spherical morphology with a particle size of 100 nm. However, the selected area

10 electron diffraction pattern (inset in Fig. 1b) confirms the amorphous nature of the

11 prepared Mg-doped NBG particles. The 10-point nitrogen adsorption–desorption

12 isotherms of the prepared Mg-doped NBG particles are given in Fig. 1c. The observed

13 results indicate that prepared particles are highly mesoporous (<50 nm), which follows

14 type IV isotherm with H1 hysteresis loops in the mesoporous range.[24] The SSA,

15 average pore diameter, and total pore volume of the Mg-doped NBG particles are,

16 104.1 m^2g^{-1}, 20.17 nm, and 0.53 cm^3g^{-1}, respectively. Similarly, the base (without

17 Mg) NBG particles also show an amorphous and agglomerated spherical morphology

18 with a particle size in the range from 100 to 150 nm.[25]

19 **Characterization of nanocomposites coated on Ti-6Al-4V and SS304 implant**

20   Fig. 2 shows the XRD pattern of pure titanium alloy (TIP), NBG-coated (TINBG),

21 and Mg-doped NBG-coated (TIMgNBG) implant before *in vitro* study. The

22 characteristic peaks observed at 35.9°, 39.1°, 40.9°, 53.7°, 64.2°, and 71.5° can be

23 assigned, respectively, to (100), (002), (101), (102), (110), and (103) crystalline nature

24 of Ti-6Al-4V (Fig. 2). Similarly, the diffraction peaks observed at 45.3° (111), 75.29°

1   (200), and 51.16° (220) in Fig. 3 correspond to crystalline nature of stainless steel

2   (SS304).

3   The amorphous NBG and Mg-doped NBG particles are successfully deposited onto

4   Ti alloy and stainless steel after spin coating, and confirms through HR-SEM analysis

5   (Fig. 4). HR-SEM images and corresponding EDX spectra of TIP, TINBG, and

6   TIMgNBG implants before *in vitro* study are shown in Fig. 4. The polished TIP shows

7   smooth surface without any scratches (Fig. 4a). The EDX pattern shows 100% purity

8   (Fig. 4a). Similarly, the pure SS304 sample also show plain smooth surface without

9   any impurities (Fig. 5a). The surfaces of the TINBG and TIMgNBG implants prepared

10 using spin-coating technique are shown in Fig. 4b and c. From the observed results it

11 is revealed that the deposition of uniform coating of particles is achieved and shows

12 slight aggregation on the coated substrate which may due to the presence of excess

13 PVP in the nanocomposite. The interface between the coating and alloy is dense, and

14 no cracks are found at the interface between titanium alloy and coating. Controlling

15 the ratio of nanobioactive glass and PVP, one can control the aggregation of bioactive

16 glass particles in PVP matrix. The EDX pattern of TIMgNBG implant confirms the

17 presence of elements such as Ti, Si, Ca, P, and Mg on the implant surface (Fig. 4c).

18 The surface morphology of the NBG- and Mg-doped NBG-coated SS304 implant

19 also shows uniform coating and smooth surface without any cracks and pores (Fig. 5).

20 These results indicate strong adherence of coating on the implant surface (Ti-6Al-4V

21 and SS304). The surface morphology of the NBG and Mg-doped NBG implants

22 became much smoother because of the PVP composite coating. The EDX pattern of

23 Mg-doped NBG-coated stainless steel implant confirms the presence of elements such

24 as Fe, Cr, Si, Ca, P, and Mg on the coated surface (Fig. 5 b and c).

1   The elemental compositions of the uncoated and coated NBG particles are

2   confirmed by XRF analysis (Table 1). The existence of elements such as Si, Ca, P, and

3   Mg on the implant surface is confirmed in NBG particles and Mg-doped NBG

4   composites. The remaining elements (Ti, V, Al, Fe, Ni, and Cr) are present in the

5   substrate. From the observed results, it is concluded that the developed

6   nanocomposite-coated implant shows negligible impurities. These results are in good

7   agreement with the observed EDX pattern.

8   AFM images of the Ti alloy (Ti-6Al-4V) and stainless steel (SS304) surface before

9   and after coatings are given in Fig 6 and 7. The two-dimensional (2D) and three-

10   dimensional (3D) views of the AFM images of polished Ti alloy and SS304 surface

11   are shown in Figs. 6a and 7a. The AFM images of the composite coated surfaces (Figs.

12   6a and 7a) show that the surface is uniform with no scratches. Figs. 6b,c and 7b,c

13   show the 2D and 3D views of Ti alloy and SS304 sample after coating of NBG- and

14   Mg-doped NBG-coated particles. Further, it confirms that an effective coating is

15   achieved by spin-coating method. In addition, the surface of the implant subjected to a

16   constant tip loading is seen in Figs. 6 and 7. It is reported that bioactive glass coating

17   on metallic implant enhances the osteoconductivity and cellular differentiation.[26]

18   However, glass composition with enhanced mechanical properties promotes the

19   stability of the implant for high load bearing applications.

20   Fig. 8 shows the potentiodynamic polarization curve of NBG particles coated on Ti-

21   6Al-4V and SS304 to explore the corrosion resistance in artificial saliva. Using Tafel

22   extrapolation method,[27, 28] the corrosion potential (E_{corr}), corrosion current density

23   (I_{corr}), anodic/cathodic Tafel (β_α and β_c), and polarization resistance (R_p) are obtained

24   from polarization curves (Fig. 8). The values of E_{corr}, I_{corr}, β_α, β_c, R_p, and corrosion rate

25   per year for NBG- and Mg-doped NBG-coated particles on Ti-6Al-4V and SS304

1   implants are given in Table 2. TINBG implant shows higher I_{corr} value of 69.4 µA

2   cm^{-2} whereas SSNBG implant shows higher I_{corr} value of 67.3 µA cm^{-2}. Similarly,

3   corrosion current densities of TIMgNBG and SSMgNBG implants were 13.5 and 9.55

4   µA cm^{-2}, respectively. From the observed results, higher I_{corr} values are evident for

5   TINBG and SSNBG when compared with those of TIMgNBG and SSMgNBG

6   implants.

7   It suggests that Mg-doped NBG-coated samples are passivated spontaneously with

8   passive current density in an artificial solution. Higher polarization resistances of

9   1415.5 and 754.99 Ω are observed for TIMgNBG and SSMgNBG implants,

10   respectively. In addition, Mg-doped NBG-coated samples show that the lower

11   corrosion rates for Ti-6Al-4V and SS304 are 0.157 and 0.111 mm/year, respectively.

12   These observed results are in good agreement with already reported studies.[28, 29] The

13   presence of bioactive glass coating improves corrosion resistance of titanium alloy and

14   stainless steel in artificial saliva solution.[29] Finally, it is concluded that the presence of

15   Mg in NBG particles improves corrosion resistance of titanium alloys and stainless

16   steels while coating and they act as a barrier that extends the lifetime of the implant.

17   The typical load–displacement curves of nanoindentation experiments for uncoated

18   and coated nanocomposites on Ti-6Al-4V and SS304 are shown in Fig. 9. From the

19   obtained curves, the hardness (H) and Young's modulus (E) values are calculated and

20   are given in Table 1. The hardness value of TIP is measured as 0.12 GPa whereas

21   those of TINBG and TIMgNBG implants are measured as 0.56 and 1.65 GPa,

22   respectively. Similarly, Young's moduli of TIP, TINBG, and TIMgNBG implants are

23   found to be 2.85, 15.72, and 12.78 GPa, respectively. In addition, the hardness value

24   of pure SS304 (SSP) is measured as 0.18 GPa whereas those of SSNBG and

25   SSMgNBG implants are measured as 0.17 and 0.75 GPa, respectively.

1   Moreover, Young's moduli of SSP, SSNBG, and SSMgNBG implants are observed

2   to be 4.48, 5.37, and 4.57 GPa, respectively. From the observed results, it is seen that

3   TIMgNBG and SSMgNBG implants show an increase in hardness and Young's

4   moduli when compared with uncoated implants. The hardness of the materials

5   determines the interfacial and intrinsic bonding of the materials for in vitro biological

6   behavior.[30] Generally, the surface roughness does not influence the immediate

7   nucleation of calcium phosphate deposits onto Ti6Al4V surfaces.[31] However, further

8   growth and mechanical attachment of the final Ca–P deposition is favoured by a

9   rougher topography rather than a smoother topography. Therefore, the Mg-doped

10   NBG coated implants with an improved anticorrosion property along with mechanical

11   stability are used for high load bearing implant applications in biomedical field.

12   *In vitro* **bioactivity evaluation**

13   The XRD patterns of the NBG- and Mg-doped NBG-coated particles on Ti-6Al-4V

14   and SS304 substrates after 21 days of immersion in SBF are shown in Fig. 10. It is

15   observed that after immersion, sharp diffraction peaks observed at 31.7° (JCPDS file

16   no. 090432) correspond to formation of the apatite layers on the surface of the coated

17   TIMgNBG and SSMgNBG implants. However, the diffraction peaks of apatite

18   deposition on TINBG and SSNBG implants are found to be very weak.

19   The apatite layer formation on the prepared implant surface after immersion in

20   SBF for 21 days is further confirmed by HR-SEM analysis and the results are shown

21   in Fig. 11. From the observed results, it is seen that Mg-doped NBG coating provides a

22   suitable surface for bone-like apatite formation. It is observed that the uncoated

23   implant immersed in SBF is different from the coated implants before and after

24   immersion in SBF. The image obtained after 21 days of SBF immersion of coated

1   implant indicates the formation of white globular apatite-like structure on the surface

2   of both Ti- and SS-coated implants. Polyvinylpyrrolidone (PVP) is known for its

3   water-soluble and biocompatible polymer properties, used in the present study to

4   induce the formation of apatite crystal.[32] PVP can effectively combine with a larger

5   amount of Ca^{2+} through a strong ion-polar interaction due to the presence of C—N and

6   C=O. The incorporated Ca^{2+} ions facilitate to combine with PO_4^{3-} and CO_3^{2-} ions in

7   SBF solution, which inturn accelerates the nucleation of HAp crystals on the implant

8   surface.[33]

9   From the observed results, it is evident that the developed Mg-doped NBG-

10 coated implants show better bioactivity and improved mechanical properties, which in

11 turn become potential glass compositions for high load-bearing applications with

12 better anticorrosion property and long-term stability. Similarly, previous observations

13 of HAp-coated implants show significant bioactivity.[16] However, the HR-SEM

14 analysis of the Mg-doped NBG-coated implant shows better HAp layer formation on

15 the implant surface.

16   From the *in vivo* cytotoxicity evaluation results, it is observed that hatching rate

17 and touch response of the zebrafish are similar in control and in the NBG-treated

18 samples (Table 3). No delay in hatching is observed for control and the NBG samples

19 tested at 100 µg mL^{-1}. However, the mortality rate is reduced by 20% in the NBG-

20 treated samples than control while observing under a microscope (Fig. 12). The

21 treatment of metal oxide nanoparticles at a concentration above 50 µg mL^{-1} causes a

22 decrease in hatching rate as well as an increase in the percentage of mortality.[23] The

23 toxic response of MgO-doped NBG particles for *in vitro* cytotoxicity evaluation

24 against human AGS cell line[21] is closely related to that for *in vivo* analysis in terms of

25 dosage effect. These observations convey that addition of optimized MgO (10%) to

1   glass matrix does not enhance cytotoxicity when compared to base glass even though

2   the addition of nanoparticles at 100 µg mL^{-1} causes stress to zebrafish, as observed

3   from Fig. 12, due to surface functionalization of particles and their binding affinity for

4   biological molecules.[34,35] Thus, rapid *in vivo* cytotoxicity screening results indirectly

5   point out the benefits associated with humans while applying the MgO-doped glass

6   particles for implant and other clinical applications.

7   **Conclusions**

8   Mg-doped NBG particles were prepared by a simple sol–gel process, mixed

9   with PVP and deposited to achieve a uniform coating on a Ti alloy and a stainless steel

10   substrate using spin-coating technique. The *in vivo* toxicity of Mg-doped NBG

11   particles showed better biocompatibility against zebrafish embryos. Electron

12   microscopic observations of Mg-doped NBG-coated Ti-6Al-4V and SS304 implants

13   indicated uniform coating achieved without cracks or micropores on the surface.

14   Compared with TIP and SS substrate, Mg-doped NBG-coated Ti implants showed an

15   increase in mechanical properties in terms of hardness. In addition, the results of *in*

16   *vitro* bioactivity studies gave a better HAp layer formation on the coated Ti-6Al-4V

17   and SS304 implants. The electrochemical polarization of Mg-doped NBG-coated Ti

18   implant led to higher corrosion resistance in artificial saliva when compared with base

19   glass coating. From the observed results, it can be concluded that the prepared Mg-

20   doped NBGcoated implants are better nanocomposites for high load-bearing

21   applications with good anticorrosive property and long-term stability.

22

23

24

1 **Materials and methods**

2 **Materials**

3   The implant materials such as Ti-6Al-4V (20 mm × 20 mm × 1.5 mm) and SS304 (20

4 mm × 20 mm × 1.5 mm) were obtained as per the ASI standard. The reagents such as

5 tetraethyl orthosilicate ($Si(OC_2H_5)_4$, TEOS; Sigma-Aldrich; min. 99%), triethyl phosphate

6 ($(CH_3CH_2O)_3P(O)$, TEP; HiMedia, Mumbai, India; min. 99.5%), calcium nitrate

7 ($Ca(NO_3)_2.4H_2O$; Merck; min. 98% GR), magnesium nitrate ($MgNO_3$; Merck; min. 99%

8 GR), 2 N nitric acid (HNO_3; Merck; min. 69% GR), ethanol, 1 M ammonia (Merck; min.

9 25% GR), polyvinyl pyrrolidone (PVP), 10% hydrofluoric acid, and ultrapure water (Arium

10 611UF; Sartorius AG) were used in this study. All the reagents were used as received without

11 any further purification.

12 **Preparation of Mg-doped NBG particles**

13   Mg-doped NBG particles, namely $58SiO_2–23CaO–9P_2O_5–10MgO$, were

14 synthesized using the simple, cost-effective sol–gel method.[21,36] Initially, TEOS

15 (14.025 ml) was dissolved in 1:1 ratio of ethanol and ultrapure water. Then 2 N HNO_3

16 (3 ml) was added to the solution under stirring for 30 min at room temperature. After

17 complete hydrolysis of TEOS, TEP (3.32 ml), $Ca(NO_3)_2.4H_2O$ (5.45 g), and

18 $Mg(NO_3).6H_2O$ (2.76 g) salts were dissolved separately with 2 ml distilled water. The

19 dissolved solution was added to silica solution at 30 min interval under constant

20 stirring at room temperature. After obtaining the clear solution, 1 M ammonia solution

21 was added drop-wise until the formation of gel, that is, until the solution attains a pH

22 of ~8.0. Thereafter, the obtained white gel was dried in a hot-air oven at 353 K for 6 h.

23 The dried gel was calcined at 873 K for 2 h in a muffle furnace to remove carbon and

24 nitrate impurities. The calcined samples were ground in a dry ball-mill (PM 100;

1   Retsch Corporation, Germany) at 500 rpm for 1 h to obtain fine Mg-doped NBG

2   particles.

3   **Coating of NBG- and Mg-doped NBG particles on implants**

4   Commercially purchased pure Ti-6Al-4V (20 mm × 20 mm × 1.5 mm) and

5   SS304 (20 mm × 20 mm × 1.5 mm) plates were sequentially polished using silicon

6   carbide papers (220, 400, 600, 1000, and 2000 grit) and then cleaned with double-

7   distilled water, followed by acetone and then with ethanol. Then, the samples were

8   eroded in 10% hydrofluoric acid solution for 30 s and cleaned with distilled water.

9   PVP was used as the binding agent for coating of prepared BG on the implant surface.

10   Ethanol was used as a solvent for dispersion of NBG and PVP in the ratio of 1:3

11   (wt%). All suspensions were stirred for 30 min and dispersed ultrasonically for

12   another 30 min to ensure a good homogeneous dispersion of the particles. After

13   dispersion, the glass particles were coated on Ti implant (Ti-6Al-4V) and stainless

14   steel (SS304) plates through spin-coating technique using a spin coater (Spin Module

15   SM-180-BT; Sawatec, Ruggell) with a rotating speed of 3000 rpm for 1 min. To

16   enhance the uniformity of the coating, the spin-coating process was repeated three

17   times for both samples. After every coating, the samples were dried in a hot-air oven

18   at 80 °C for 10 min.

19   **Characterization of NBG coating**

20   The structural nature of NBG-coated and uncoated on Ti implant (Ti-6Al-4V)

21   and stainless steel (SS304) plates and the HAp layer formation on implant surface

22   during *in vitro* studies were characterized by an X-ray diffractometer (X'Pert PRO;

23   PANalytical, Almelo, the Netherlands) with Cu Kα as the radiation (λ = 1.5418 Å)

24   source. The source was operated at 40 kV with 2θ value varying from 10° to 80° at a

1   step size of 0.02° and step duration of 25 s. The specific surface area (SSA) of the

2   prepared Mg-doped NBG particles was measured according to Brunauer–Emmett–

3   Teller (BET) method[37] using the BET surface area analyzer (Autosorb AS-1MP;

4   Quantachrome, USA). The sample was degassed for 3 h at 295 °C and physisorption

5   analysis was performed with N_2 adsorption measurements at liquid N_2 temperature

6   (−196 °C). Ten-point adsorption and desorption branched isotherm were used to find

7   the total pore volume, and average pore diameter of the Mg-doped NBG particles

8   using Barrett-Joyner-Halenda (BJH) method[38]. Transmission electron microscope

9   (TEM; CM 200; Philips, USA) was used to characterize particle size and surface

10 morphology of the prepared Mg-doped NBG particles.

11 Elemental compositions of the NBG-coated and uncoated Ti implant (Ti-6Al-4V)

12 and stainless steel (SS304) plates were measured by X-ray fluorescence (XRF)

13 spectrometer (EDX-720; Shimadzu, Kyoto, Japan). High-resolution scanning electron

14 microscope (HR-SEM) equipped with energy-dispersive X-ray analysis (EDX)

15 (Quanta FEG 200; FEI, the Netherlands) was used to explore the difference in surface

16 morphology and composition of the NBG-coated and uncoated substrates. The

17 substrates were examined at an accelerating voltage of 30 kV. The elemental wt% was

18 calculated using ZAF program of the EDX system. The topography of the NBG-

19 coated and uncoated samples was analyzed through atomic force microscopy (AFM;

20 version 7; Innova, USA) in contact mode using a Si_3N_4 cantilever with a spring

21 constant of about 34 Nm^{-1} and a resonance frequency of about 200 kHz. Scanning was

22 performed at a scan speed of 0.5 Hz with a resolution of 256 × 256 pixels. The tip

23 loading force was controlled to avoid structural changes in the sample.

24 The mechanical properties such as Young's modulus and hardness of the NBG-coated

25 and uncoated samples were measured using the quasistatic nanoindentation (TI 700

1 Ubi; Hysitron, USA) system. The indentation was performed by applying a force in

2 the range of 100 Nn to 10 N on the sample using a transducer, and the displacement

3 with respect to depth force was observed. The hardness, H, of the material was

4 measured using the following formula:

$$H = \frac{P_{max}}{A}$$

5 (i)

6 where P_{max} is the maximum applied load and A the projected area. The slope (S) of the

7 unloading curve provides a measure of the contact stiffness, which can be used with

8 the contact area to determine the elastic modulus.[39] The elastic modulus (E_r) of the

9 prepared material was measured using the following formula:

$$E_r = \frac{\sqrt{\pi}}{2\sqrt{A}} S$$

10 (ii)

11 where S is the slope of the curve and A the selected area of the sample.

12 **Electrochemical corrosion behaviour**

13 The electrochemical corrosion resistance of the NBG-coated Ti implants (Ti-6Al-

14 4V) and stainless steel (SS304) plates was measured using artificial saliva at room

15 temperature. Artificial saliva was prepared with a pH value of 6.8 as mentioned by Gal

16 *et al.*[27]; the composition of the artificial saliva is given in Table 4. A stainless steel and

17 a saturated calomel electrode were used as the counter and the reference electrode,

18 respectively. The sample was taken as working electrode having a test surface area of

19 1 cm^2 for all experiments. Linear polarization measurement was performed using

20 PGSTAT 362N (Autolab, the Netherlands) device in a three-electrode cell with a scan

21 rate of 1 mV s^{-1}. The corrosion potential (E_{corr}), corrosion current density (I_{corr}), and

22 polarization resistance (R_p) were calculated from the Tafel pl

1

2   *In vitro* **bioactivity study**

3   The *in vitro* bioactivity of the NBG-coated Ti implant (Ti-6Al-4V) and

4   stainless steel (SS304) was measured using freshly prepared SBF. The SBF was

5   prepared using standard protocol[40] wherein the pH value was maintained as 7.4, which

6   was equivalent to that of human blood plasma. Each coated substrate was placed

7   separately in polyurethane bottle containing 50 ml SBF and was then incubated at 37

8   °C for 21 days. After 21 days of incubation, the coated substrates were removed from

9   the SBF and then washed gently with distilled water. The washed coated substrates

10 were dried at 100 °C for 1 h, which were then used for further characterization studies

11 such as X-ray diffraction (XRD) and SEM to study the HAp layer formation on the

12 coated surface.

13 *In vivo* **toxicity studies**

14   The suspensions of glass samples were made to study the *in vivo* toxicity. Base

15 glass and MgO-doped NBG particles were weighed and then suspended in water to

16 prepare a working solution (100 μg mL^{-1}) using egg water (sea salt). Eggs of wild-

17 type zebrafish were collected, washed 2–3 times with water, and then transferred to

18 egg water. Nanotoxicity studies using zebrafish embryos were carried out per the

19 procedure reported by Asharani *et al.*[23] Ten healthy embryos (eight-cell stage) were

20 transferred to each well of 12-well plates. The embryos were treated with 100 μg mL^{-1}

21 of the glass samples dispersed in egg water and were observed at specific growth

22 stages for various criteria such as mortality, rate and time of hatching, development of

23 organs, touch responses, and edema. The dead embryos were removed immediately

24 from the medium during the observation period and the remaining embryos were

1   counted. The touch response of the larvae was tested by gently touching the sides of

2   the trunk with a smooth pipette tip. At the end of the experiment, the larvae were

3   transferred to a microscope slide and then anesthetized with 0.1% phenoxyethanol.

4   Microscopic observations were performed using a Zeiss Axiovert 200M microscope

5   equipped with Axiocam HRc to determine the mortality of the treated embryos.

6   **Acknowledgements**

10   **References**

1   M.H. Fathi and A. Doostmohammadi, *Journal of Materials Processing Technology,*
     2009, **209**, 1385.

2   M. Mehdikhani-Nahrkhalaji, M.H. Fathi, V. Mortazavi, S.B. Mousavi, B.
     Hashemi-Beni and S.M. Razavi, *Journal of Material Science. Materials in
     Medicine*, 2012, **23**, 485.

3   V.R. Noort. *Journal of Materials Science*, 1987, **22**, 3801.

4   F. Bir, H. Khireddine, A. Touatib, D. Sidane, S. Yala and H. Oudadesse, *Applied
     Surface Science,* 2012, **258**, 7021.

5   A. Rakngarm and Y. Mutoh. *Materials Science and Engineering C,* 2009, **29**, 275.

6   X. Bai, S. Sandukas, M.R. Appleford, J.L. Ong and A. Rabiei. *Acta Biomaterelia,*
     2009, **5**, 3563.

7   X.-H. Xie, X.-W. Yu, S.-X. Zeng, R.-L. Du, Y.-H. Hu, Z. Yuan, E.-Y. Lu, K.-R.
     Dai and T.-T. Tang, *Journal of Material Science. Materials in Medicine*, 2010,
     21, 2165.

8   A. de Carlos, J.P. Borrajo, J. Serra, P. González and B. Léon, *Journal of Material
     Science. Materials in Medicine*, 2006, **17,** 523.

9   N. Lotfibakhshaiesh, D.S. Brauer and R.G. Hill, *Journal of Non-Crystalline
     Solids,* 2010, **356,** 2583.

10   S. Bharati, C. Soundrapandian, D. Basu and S. Datta, *Journal of European
     Ceramic Society,* 2009, **29,** 2527.

11   L. Floroian, F. Sima, M. Florescu, M. Badea, A.C. Popescu, N. Serban and I.N. Mihailescu, *Journal of Electroanalytical Chemistry*, 2010, **648,** 111.

12   L. Floroian, M. Florescu, F. Sima, G. Popescu-Pelin, C. Ristoscu and I.N. Mihailescu, *Materials Science and Engineering C,* 2012, **32,** 1152.

13   X. Liu, S. Tao and C. Ding, *Biomaterials,* 2002, **23,** 963.

14   L. D'Alessio, R. Teghil, M. Zaccagnino, I. Zaccardo, D. Ferro and V. Marotta, *Applied Surface Science,* 1999, **138–139**, 527.

15   S. Sutha, G. Karunakaran and V. Rajendran, *Ceramics International,* 2013, **39**, 5205.

16   S. Sutha, K. Kavitha, G. Karunakaran and V. Rajendran, *Materials Science and Engineering C,* 2013, **33,** 4046.

17   N. Drnovšek, S. Novak, U. Dragin, M. Čeh, M. Gorenšek and M. Gradišar, International Orthopaedics (SICOT) 2012, **36,** 1739.

18   R.Y. Whitehead, W.R. Lacefield and L.C. Lucas. *Journal of Biomedical Materials Research,* 1993, **27,** 1501.

19   G. Koller, R. Cook, I. Thompson, T. Watson and L. DiSilvio*, Journal of Material Science. Materials in Medicine*, 2007, **18,** 2291.

20   Z. Ma, H. Ji, X. Hu, Y. Teng, G. Zhao, L. Mo, X. Zhao, W. Chen, J. Qiu and M. Zhang. *Applied Surface Science,* 2013, **284,** 738.

21   M. Prabhu, K. Kavitha, P. Manivasakan, V. Rajendran, P. Kulandaivelu. *Ceramics International*, 2013, **39**, 1683.

22   M. Prabhu, K. Kavitha, R. Suriyaprabha, P. Manivasakan, V. Rajendran and P. Kulandaivelu. *Journal of Nanoscience and Nanotechnology,* 2013, **13,** 5327.

23   P.V. Asharani, Y. Lianwu, Z. Gong and S. Valiyaveettil, *Nanotoxicology*, 2011, **5(1),** 43.

24   J.H. De Boer, in D.H. Everett and F.S. Stone (editors) Butterworths, UK, 1958, 68.

25   B. Saravanakumar, M. Prabhu and V. Rajendran., *International Journal of Applied Ceramic Technology,* 2013, doi: 10.1111/ijac.12124.

26   R. Gupta and A. Kumar, *Biomedical Materials*, 2008, **3**, 034005.

27   J.-Y. Gal, Y. Fovet and M. Adib-Yadzi, *Talanta,* 2001, **53,** 1103.

28   I. Gurappa, *Surface and Coating Technology*, 2002, **161**, 70.

29   M. Mehdipour, A. Afshar and M. Mohebali, *Applied Surface Science*, 2012, **258**, 9832.

30   J.M. Gomez-Vega, E. Saiz, A.P. Tomsia, G.W. Marshall and S.J. Marshall, *Biomaterials*, 2000, **21**, 105.

31   A. Arvidsson, V. Franke-Stenport, M. Andersson, P. Kjellin, Y.T. Sul and A. Wennerberg, *Journal of Materials Science. Materials in Medicine*, 2007, **18**, 1945.

32   I.S. Elashmawi and H.E. Abdel Baieth, *Current Applied Physics*, 2012, **11**, 141.

33   N. Yin, S.Y. Chen, Y. Ouyang, L. Tang, J.X. Yang and H.P. Wang, *Progress in Natural Science: Materials International*, 2011, **21**, 472.

34   T. Cedervall, I. Lynch, S. Lindman, T. Berggard, E. Thulin, H. Nilsson, K.A. Dawson and S. Linse. *Proceedings of National Academy of Sciences*, USA, 2007, **104,** 2050.

35   A. Villanueva, M. Canete, A.G. Roca, M. Calero, S. Veintemillas-Verdaguer, C.J. Serna, M.P. Morales and R. Miranda. *Nanotechnology*, 2009, **20,** 115103.

36   W. Xia and J. Chang, *Materials Letter,* 2007, **61,** 3251.

37   S. Brunauer, P.H. Emmett and E. Teller, Journal of American Chemical Society, 1938, **60**, 309.

38   E.P. Barrett, L.G. Joyner, and P.P. Halenda, Journal of American Chemical Society, 1951, **73**, 373.

39   H.H. Xu, D.T. Smith and C.G. Simon, *Biomaterials,* 2004, **25,** 4615.

40   T. Kokubo and H. Takadama, *Biomaterials*, 2006, **27,** 2907.

1

2

3

4

5

6

7

8

9

10

11

12

1   **Figure Captions**

2

3   **Fig. 1.** Characterization of MgO-doped bioactive glass nanoparticles

4

5   **Fig. 2.** XRD patterns of NBG- and Mg-doped NBG-coated and un-coated titanium alloy (Ti-

6   6Al-4V) implants

7

8   **Fig. 3.** XRD patterns of NBG- and Mg-doped NBG-coated and uncoated stainless steel

9   (SS304) implants

10

11   **Fig. 4.** HR-SEM images of NBG- and Mg-doped NBG-coated and uncoated titanium alloy

12   (Ti-6Al-4V) implants

13

14   **Fig. 5.** HR-SEM images of NBG- and Mg-doped NBG-coated and un-coated stainless steel

15   (SS304) implants

16

17   **Fig. 6.** AFM images of NBG- and Mg-doped NBG-coated and un-coated Ti-6Al-4V implants

18

19   **Fig. 7.** AFM images of NBG- and Mg-doped NBG-coated and uncoated stainless steel

20   (SS304) implants

21

22   **Fig. 8.** Potentiodynamic polarization curve of the NBG- and Mg-doped NBG-coated Ti-6Al-

23   4V and SS304 implants in artificial saliva

24

25   **Fig. 9.** Typical load–displacement curve of the nanocomposite-coated and uncoated Ti-6Al-

26   4V and SS304 implants

27

28   **Fig. 10.** XRD patterns of the nanocomposites-coated Ti-6Al-4V and SS304 substrates after

29   21 days of immersion in SBF

30

31   **Fig. 11.** HR-SEM images of the nanocomposites-coated Ti-6Al-4V and SS304 substrates

32   after 21 days of immersion in SBF

33

34   **Fig. 12.** *In vivo* analysis of the prepared nanocomposites using zebrafish (*D. rerio*) embryos

35

36

37

38

39

40

41

42

43

Table 1 Elemental composition and mechanical properties of magnesium doped nanobioactive glass coated implant confirmed through XRF analysis and Nano indentation techniques

Sample	Element (Wt%)										Mechanical properties	
	Ti	Al	V	Fe	Cr	Ni	Si	Ca	P	Mg	Hardness (GPa)	Young's Modulus (GPa)
TIP	88.52	7.46	2.62	1.40	-	-	-	-	-	-	0.12	2.85
TINBG	84.18	-	2.96	0.17	-	-	8.68	2.40	1.59	-	0.56	15.72
TiMgNBG	82.91	-	3.50	-	-	-	8.37	3.57	1.41	0.24	1.65	12.78
SSP	-	-	-	70.42	19.54	07.56	01.59	-	-	-	0.18	4.48
SSNBG	-	-	-	56.52	16.03	5.90	12.67	6.63	2.19	-	0.17	5.37
SSMgNBG	-	-	-	56.66	15.71	6.22	11.18	7.03	2.10	0.94	0.75	4.57

Table 2 Corrosion parameters from the potentiodynamic polarization test for NBG and Mg-NBG   coated sample in artificial saliva

Sample	Ecorr (V)	Icorr ($\mu A\ cm^{-2}$)	$\beta\alpha$ (V/decade)	βc (V/decade)	Polarisation resistance (Rp) (Ω)	Corrosion rate (mm/year)
TINBG	-0.620	69.4	0.123	0.127	391.86	0.806
TIMgNBG	-0.534	13.5	0.098	0.080	1415.5	0.157
SSNBG	-0.635	67.3	0.119	0.126	396.6	0.782
SSMgNBG	-0.614	9.55	0.038	0.028	754.99	0.111

1

2

3

4

5

6

7

8

9

10

1   Table 3 *In vivo* toxicity of zebrafish embryos treated with bioactive glass samples

Stages of embryos	Control		NBG		MgNBG	
(Nos)	After 48 h	After 72 h	After 48 h	After 72 h	After 48 h	After 72 h
Hatched embryos (N/Ab)	0/0	10/0	3/0	9/0	2/1	1/7
Unhatched embryos (N/Ab)	10/0	0	1/5	0	1/4	0
Dead embryos	0	0	1	1	2	2

2   N - normal, Ab – abnormal

3

4

5

6

7

8

9

10

11

12

13

14

15

16

1   Table 4 Composition of artificial saliva solution

Compound	Concentration (mg L^{-1})	Compound	Concentration (mg L^{-1})
NaCl	125.6	Na$_2$SO$_4$·10H$_2$O	763.2
NH$_4$Cl	178	KSCN	189.2
KCl	963.9	KH$_2$PO$_4$	654.5
NaHCO$_3$	630.8	CaCl$_2$·2H$_2$O	227.8
Urea	200		

2

3

4

5

6

7

8

9

10

11

12

13

14
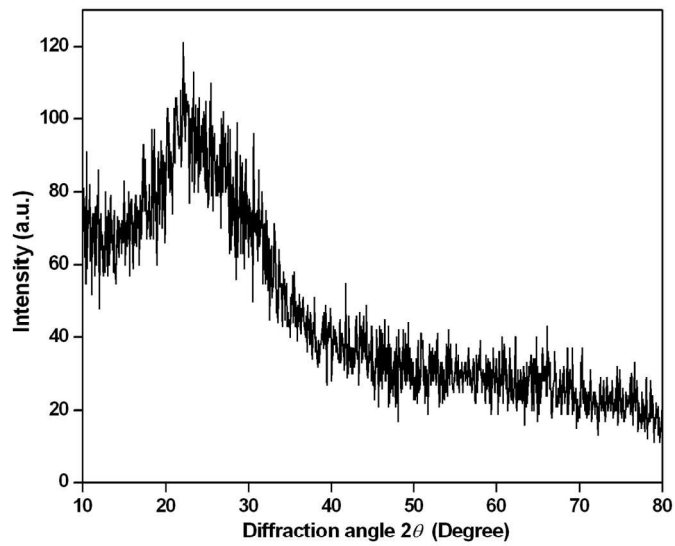
a) XRD pattern
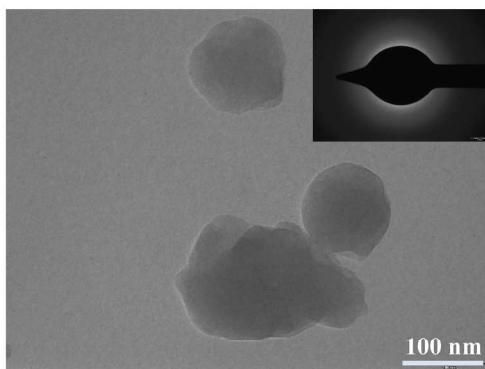
b) TEM
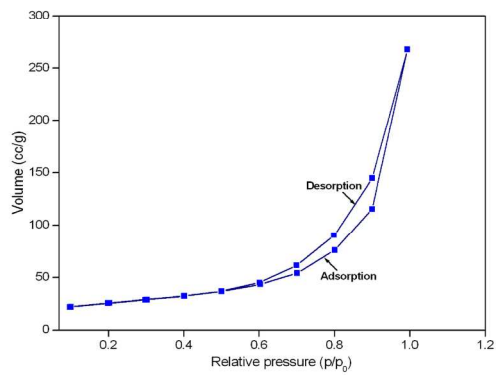
c) BET- Adsorption-Desorption Isotherm

177x189mm (300 x 300 DPI)
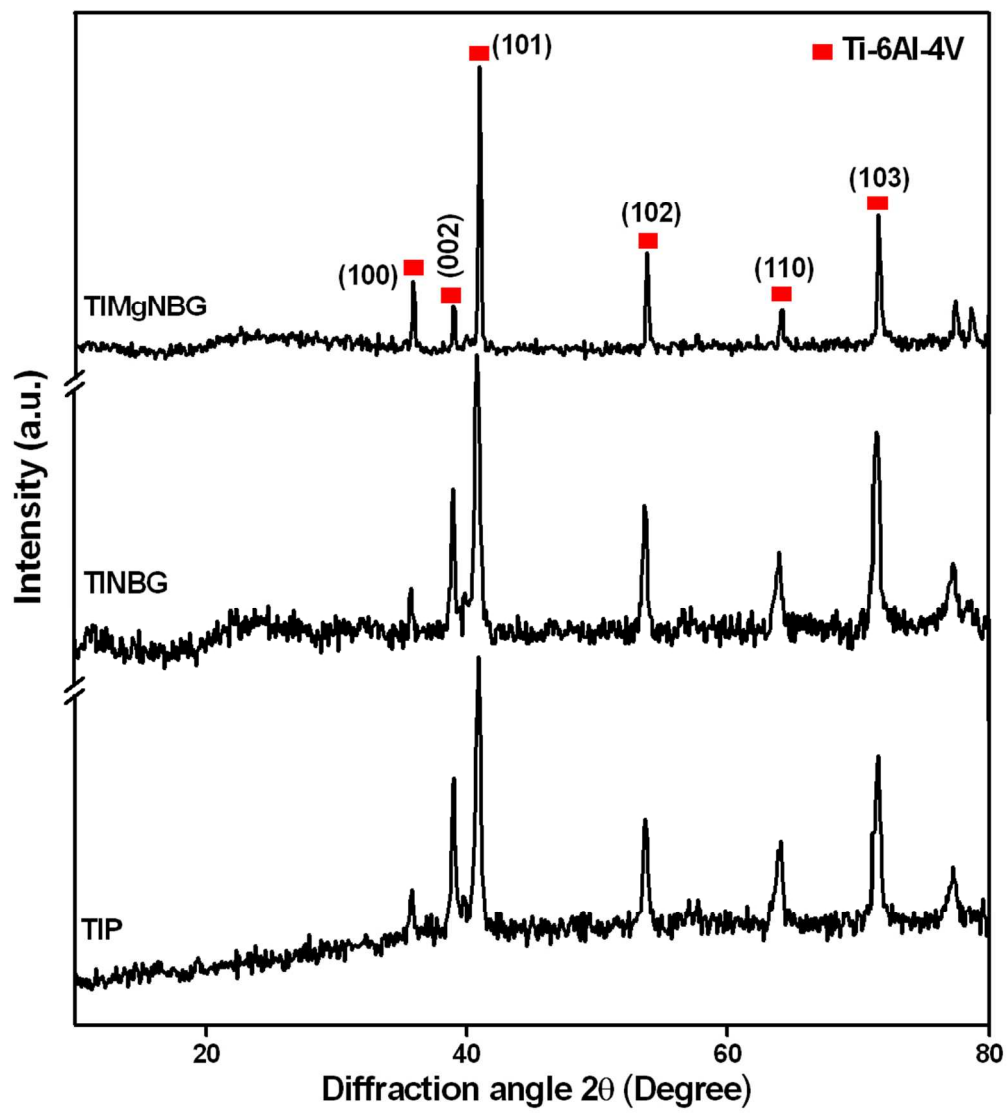
186x207mm (150 x 150 DPI)

158x166mm (150 x 150 DPI)

Element	Weight %
Ti	89.66
V	03.21
Al	07.12

i) HR-SEM image   ii) EDX pattern

a) Pure Ti alloy (TIP)

Element	Weight %
C	68.95
Ti	12.90
O	08.38
Si	04.24
P	00.90
Ca	02.87
Al	0.40
Au	01.36

i) HR-SEM image   ii) EDX pattern

b) NBG coated Ti alloy (TINBG)

Element	Weight %
C	45.73
Ti	45.67
O	07.23
Si	0.38
P	00.22
Ca	00.26
Mg	0.50
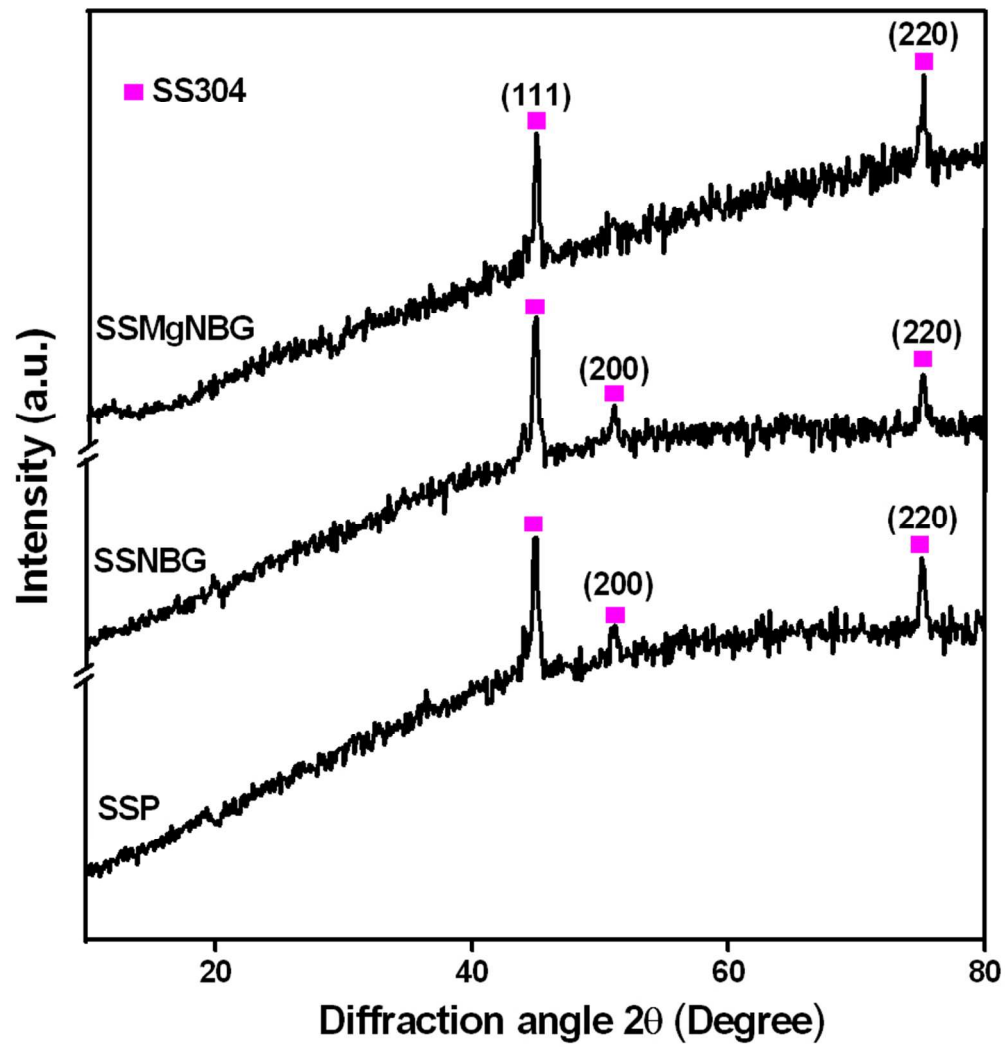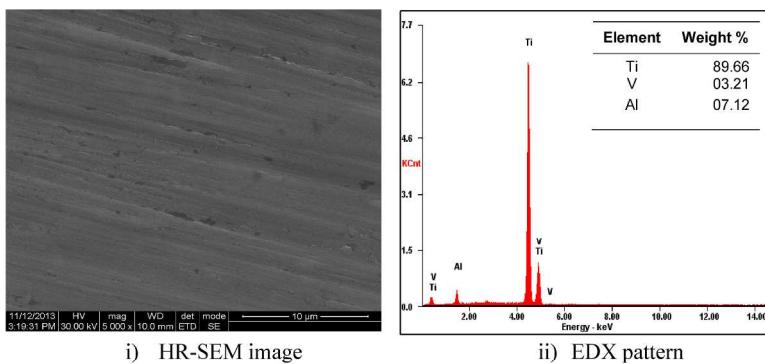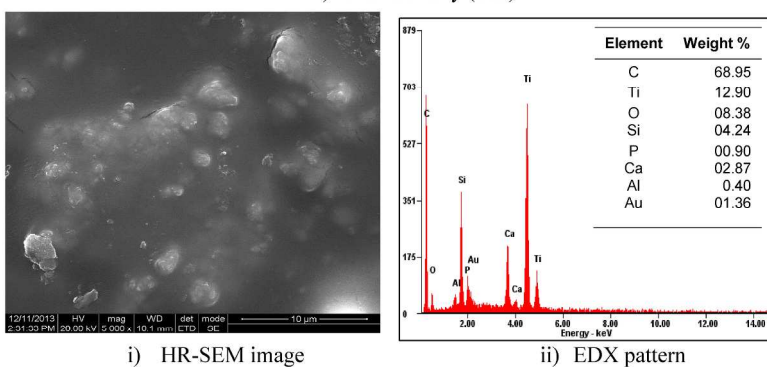
i) HR-SEM image   ii) EDX pattern
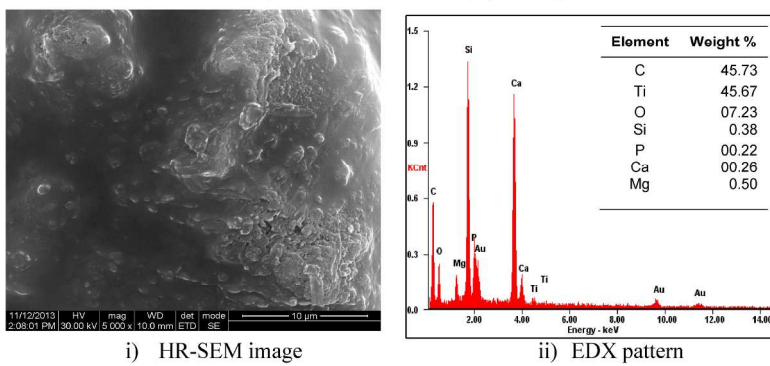
c) Mg NBG coated Ti alloy (TIMgNBG)

222x329mm (300 x 300 DPI)
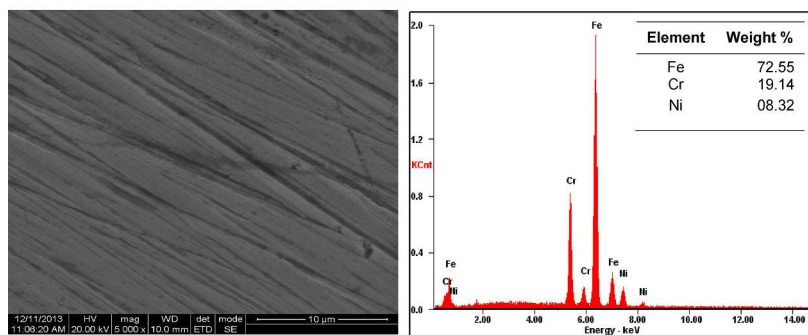
i) HR-SEM image   ii) EDX pattern

a) Pure SS304 (SSP)
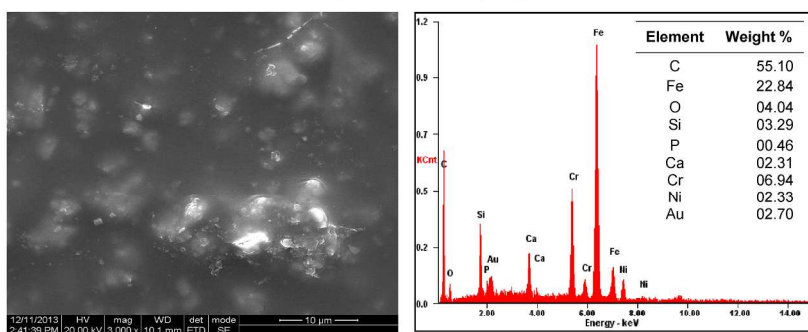
i) HR-SEM image   ii) EDX pattern

b) NBG coated SS304 (SSNBG)
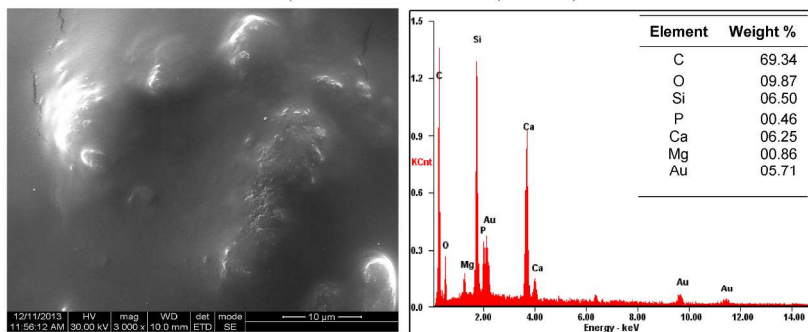
i) HR-SEM image   ii) EDX pattern

c) Mg NBG coated SS304 (SSMgNBG)

220x315mm (300 x 300 DPI)
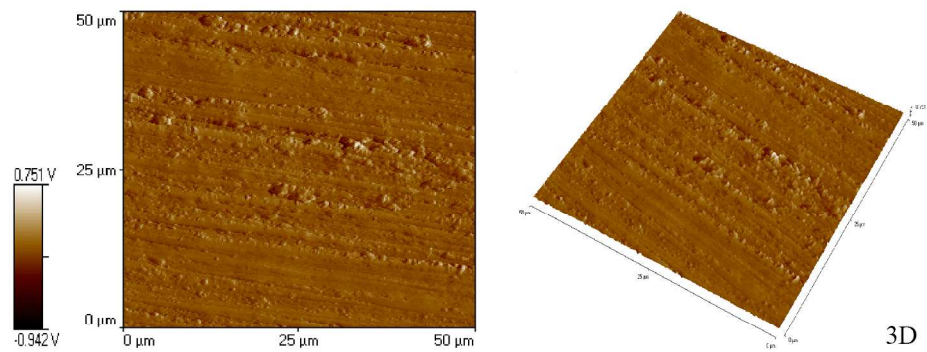
a) TIP
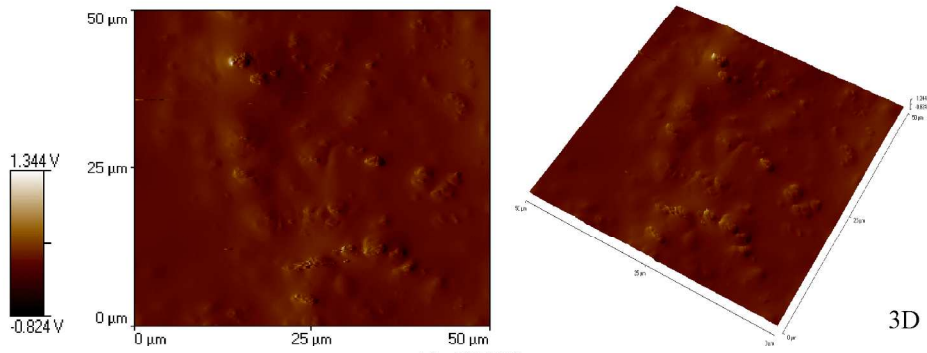
b) TINBG
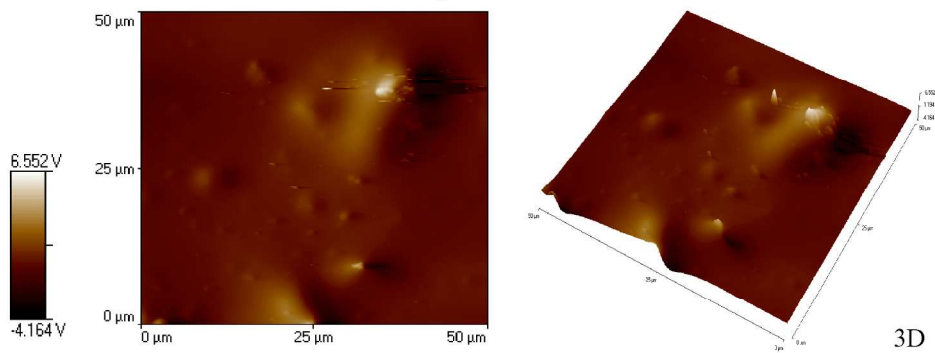
c) TIMgNBG

184x228mm (300 x 300 DPI)
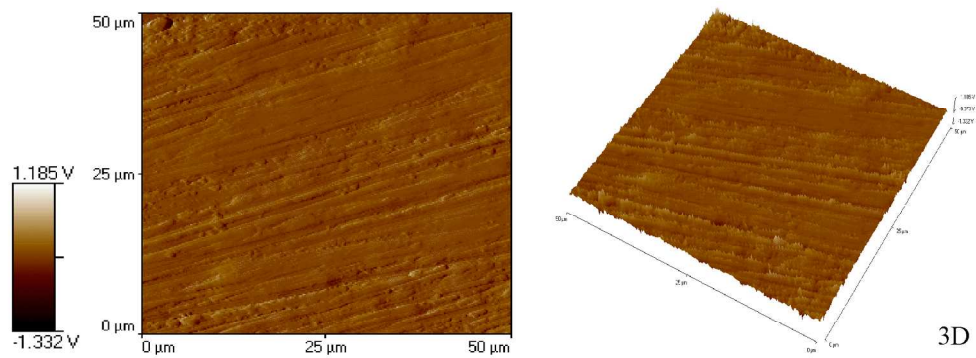
a) SSP
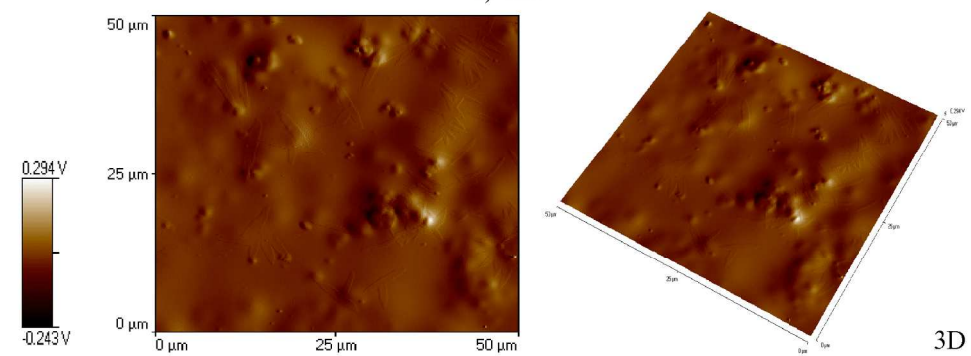
b) SSNBG
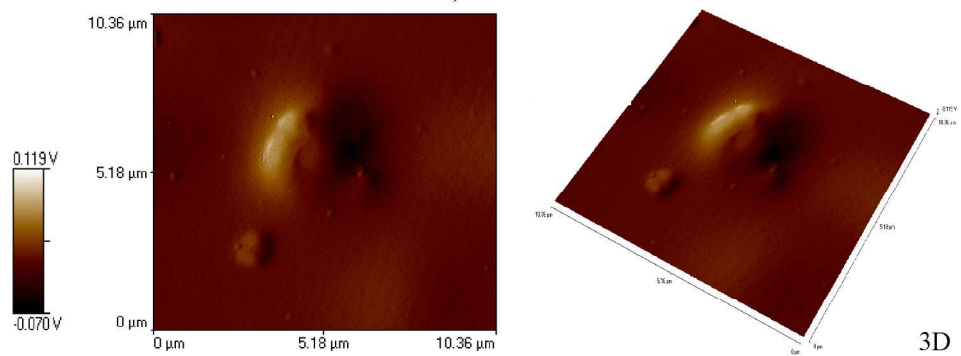
c) SSMgNBG

188x220mm (300 x 300 DPI)
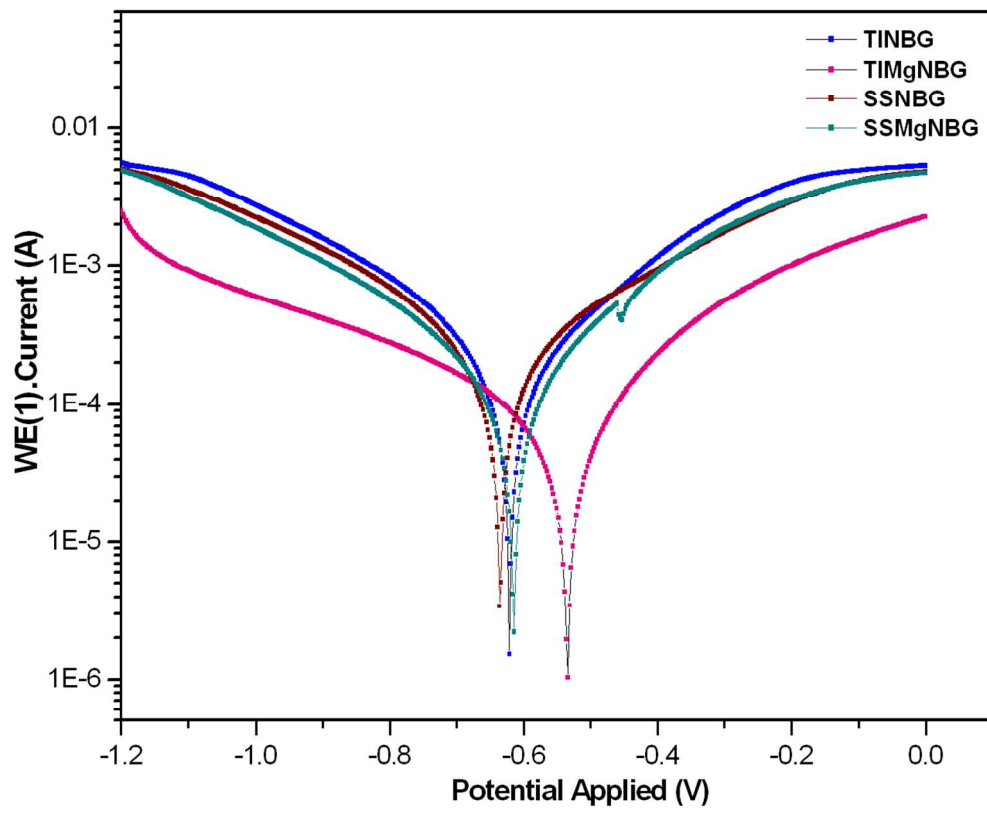
219x178mm (150 x 150 DPI)
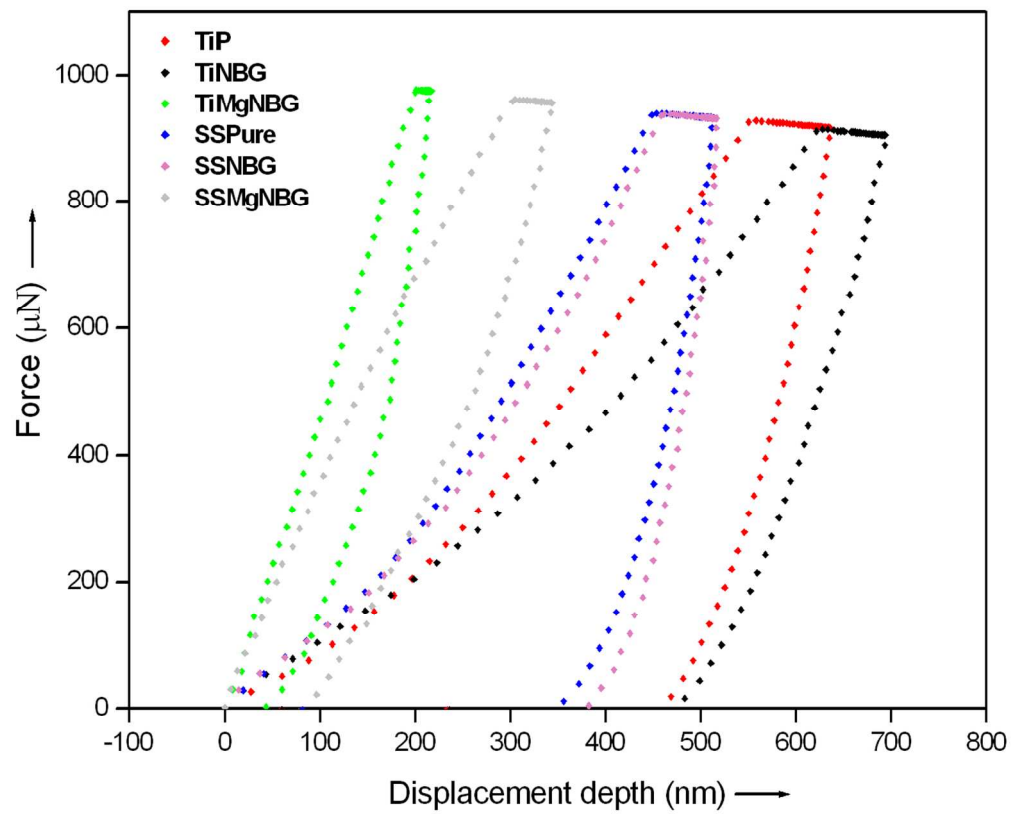
222x182mm (150 x 150 DPI)
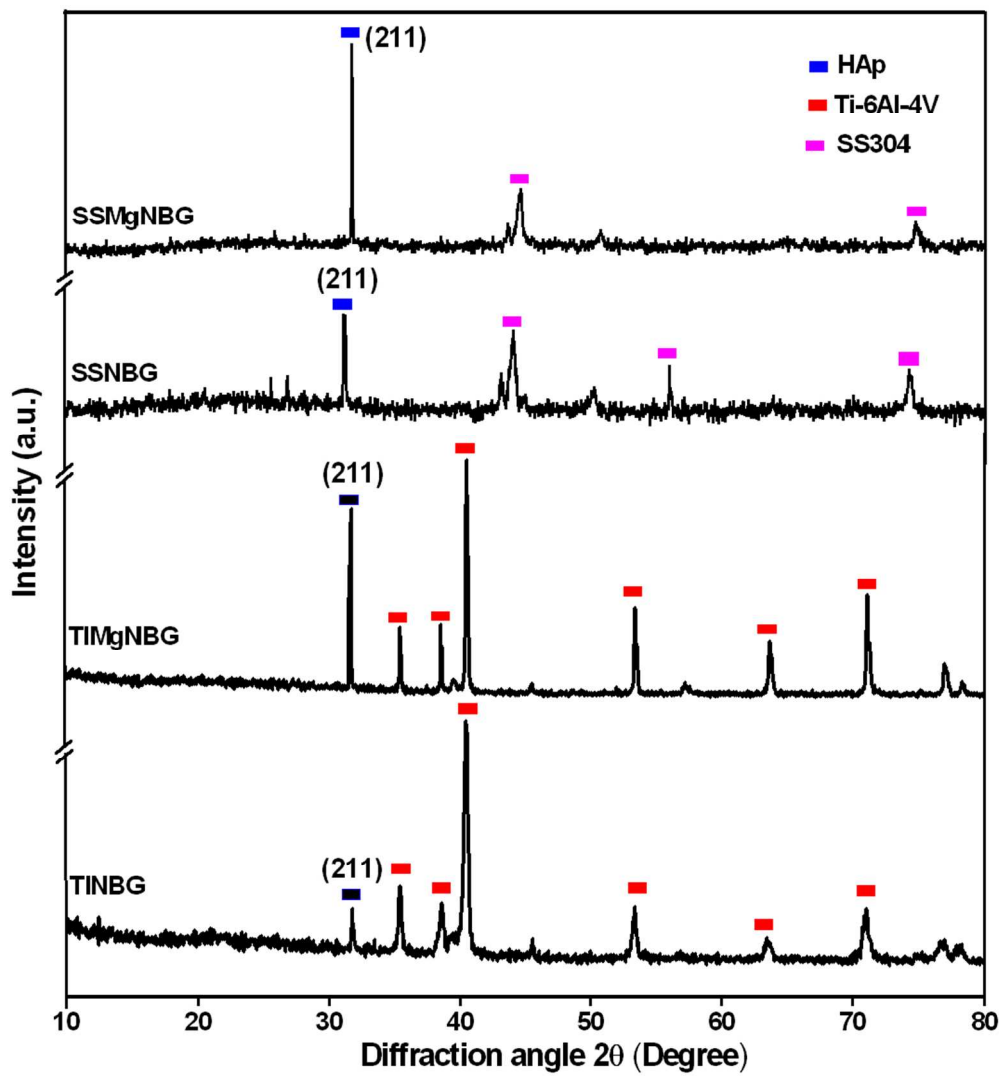
182x195mm (150 x 150 DPI)
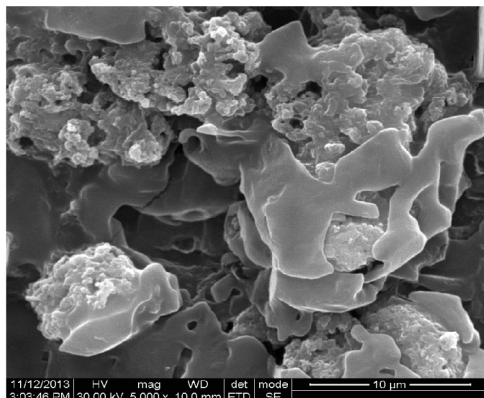
a) TINBG
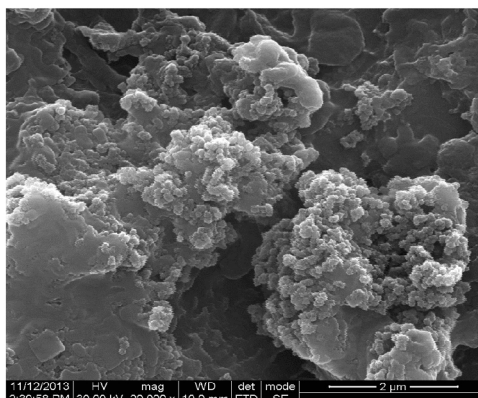
b) TIMgNBG
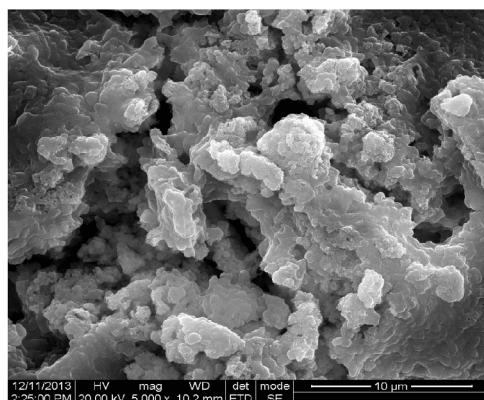
c) SSNBG
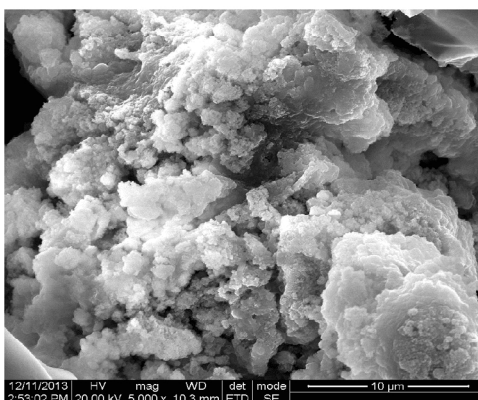
d) SSMgNBG

165x150mm (300 x 300 DPI)

i) After 48 h   ii) After 72 h

a) Control

i) After 48 h   ii) After 72 h

b) NBG particles

i) After 48 h   ii) After 72 h

c) Mg doped NBG particles

217x288mm (300 x 300 DPI)